frontiers | Frontiers in Physics

TYPE Original Research
PUBLISHED 09 January 2023
DOI 10.3389/fphy.2022.1055401

OPEN ACCESS

EDITED BY
Muhsin Caner Gokce,
TED University, Turkey

REVIEWED BY
Serkan Sahin,
TED University, Turkey
Guoquan Zhou,
Zhejiang Agriculture and Forestry University, China

*CORRESPONDENCE
Milo W. Hyde IV,
milo.hyde@afit.edu

SPECIALTY SECTION
This article was submitted to Optics and Photonics,
a section of the journal
Frontiers in Physics

RECEIVED 27 September 2022
ACCEPTED 02 December 2022
PUBLISHED 09 January 2023

CITATION
Hyde IV MW (2023), The behavior of partially coherent twisted space-time beams in atmospheric turbulence.
Front. Phys. 10:1055401.
doi: 10.3389/fphy.2022.1055401

The behavior of partially coherent twisted space-time beams in atmospheric turbulence

Milo W. Hyde IV*

Department of Engineering Physics, Air Force Institute of Technology, Dayton, OH, United States

We study how atmospheric turbulence affects twisted space-time beams, which are non-stationary random optical fields whose space and time dimensions are coupled with a stochastic twist. Applying the extended Huygens–Fresnel principle, we derive the mutual coherence function of a twisted space-time beam after propagating a distance z through atmospheric turbulence of arbitrary strength. We specialize the result to derive the ensemble-averaged irradiance and discuss how turbulence affects the beam's spatial size, pulse width, and space-time twist. Lastly, we generate, in simulation, twisted space-time beam field realizations and propagate them through atmospheric phase screens to validate our analysis.

KEYWORDS

atmospheric turbulence, coherence, random media, random fields, space-time coupling, spatiotemporal coupling, statistical optics

1 Introduction

New approaches in beam control include light with engineered space-time or spatiotemporal coupling. Recent papers have demonstrated space-time-coupled light which exhibits anomalous diffractive and refractive behaviors [1–4] as well as carries transverse (to the direction of propagation) orbital angular momentum in the form of spatiotemporal optical vortices (STOVs) [5–11]. These novel developments hold promise for exciting advancements in applications such as optical communications, optical tweezing, and quantum optics [2, 4, 12–16].

Most of the space-time-coupled beam research manipulates coherent light, although this has begun to change with the development of partially coherent STOV and twisted space-time (and space-frequency) beams [17–21]. The latter are non-stationary random fields with the beams' spatial and temporal (or spectral) dimensions coupled in a stochastic twist. They are the spatiotemporal counterparts of traditional, spatially twisted Gaussian Schell-model beams [22–27].

Spatially twisted partially coherent fields have been extensively studied since being introduced in 1993. This research includes beam synthesis [28–33]; coherent modes/pseudo-modes [23, 26, 27, 34–37]; angular momentum [38–41]; and propagation behaviors in free-space, *ABCD* optical systems, and turbulence [35, 42–51]. This stands in contrast to twisted space-time beams (and STOV beams more generally), where only their angular momentum and free-space propagation behaviors have been investigated [6, 8, 9, 11, 19, 20, 52, 53].

In this paper, we undertake, to our knowledge, the first study on the effects of atmospheric turbulence on twisted space-time beams. Using the extended Huygens–Fresnel principle, we derive an approximate expression for the mutual coherence function (MCF) of a twisted space-time beam after propagating through atmospheric turbulence of any strength. We then specialize the MCF to obtain the ensemble-averaged irradiance and discuss how turbulence affects the beam's size, pulse width, and space-time twist. To validate our analysis, we compare the theoretical irradiance to the results of Monte Carlo wave-optics simulations. Lastly, we conclude with a brief summary of our findings.

2 Theory

2.1 Extended Huygens–Fresnel principle

Let us begin with the extended Huygens–Fresnel principle/integral:

$$U(\boldsymbol{\rho}, z, \omega) = \frac{k}{\mathrm{j}2\pi z}\exp(\mathrm{j}kz)\iint_{-\infty}^{\infty} U(\boldsymbol{\rho}', 0, \omega)\exp\left(\frac{\mathrm{j}k}{2z}|\boldsymbol{\rho}-\boldsymbol{\rho}'|^2\right) \exp[\Psi(\boldsymbol{\rho}', 0; \boldsymbol{\rho}, z; \omega)]\mathrm{d}^2\rho', \tag{1}$$

where $\mathrm{j} = \sqrt{-1}$, ω is the radian frequency, $k = \omega/c$ is the wavenumber, c is the speed of light, $\boldsymbol{\rho}' = \hat{\boldsymbol{x}}x' + \hat{\boldsymbol{y}}y'$ is the source vector, and $\boldsymbol{\rho} = \hat{\boldsymbol{x}}x + \hat{\boldsymbol{y}}y$ is the observation vector. The optical field U in the integrand is a stochastic (frequency-domain) realization of a twisted space-time beam, and Ψ is a random complex function which models the phase and amplitude fluctuations of a point source propagating through atmospheric turbulence from $(\boldsymbol{\rho}', 0)$ to $(\boldsymbol{\rho}, z)$ at frequency ω [54–57].

The two-frequency cross-spectral density (CSD) function [55, 58–62] can be obtained by taking the ensemble-averaged auto-correlation of Eq. 1, namely,

$$\begin{aligned} &W(\boldsymbol{\rho}_1, z, \omega_1, \boldsymbol{\rho}_2, z, \omega_2) \\ &= \frac{k_1k_2}{(2\pi)^2z^2}\exp[\mathrm{j}(k_1-k_2)z]\iiiint_{-\infty}^{\infty} W(\boldsymbol{\rho}_1', 0, \omega_1, \boldsymbol{\rho}_2', 0, \omega_2) \\ &\exp\left(\frac{\mathrm{j}k_1}{2z}|\boldsymbol{\rho}_1-\boldsymbol{\rho}_1'|^2\right)\exp\left(-\frac{\mathrm{j}k_2}{2z}|\boldsymbol{\rho}_2-\boldsymbol{\rho}_2'|^2\right) \\ &\langle\exp[\Psi(\boldsymbol{\rho}_1', 0; \boldsymbol{\rho}_1, z; \omega_1) + \Psi^*(\boldsymbol{\rho}_2', 0; \boldsymbol{\rho}_2, z; \omega_2)]\rangle\mathrm{d}^2\rho_1'\mathrm{d}^2\rho_2', \end{aligned} \tag{2}$$

where we have assumed that the source field is statistically independent of the atmospheric turbulence fluctuations. The moment involving Ψ is related to the two-point, spherical wave structure function (WSF) [55–57, 61, 62], and equals

$$\begin{aligned} &\langle\exp[\Psi(\boldsymbol{\rho}_1', 0; \boldsymbol{\rho}_1, z; \omega_1) + \Psi^*(\boldsymbol{\rho}_2', 0; \boldsymbol{\rho}_2, z; \omega_2)]\rangle \\ &= \exp\left[-\frac{1}{2}D(\boldsymbol{\rho}_1'-\boldsymbol{\rho}_2', 0; \boldsymbol{\rho}_1-\boldsymbol{\rho}_2, z; \omega_1, \omega_2)\right] \\ &\approx \exp\left\{-2\pi^2\int_0^z\int_0^\infty \kappa\Phi_n(\kappa, \zeta)\left[k_1^2+k_2^2-2k_1k_2\exp(-\mathrm{j}\beta\kappa^2)J_0(\kappa R)\right]\mathrm{d}\kappa\mathrm{d}\zeta\right\}, \end{aligned} \tag{3}$$

where Φ_n is the index of refraction power spectrum (assumed to be statistically isotropic) and β and R equal

$$\begin{aligned} \beta &= \frac{\zeta(z-\zeta)}{2z}\left(\frac{1}{k_1}-\frac{1}{k_2}\right) \\ R &= \left|\frac{\zeta}{z}(\boldsymbol{\rho}_1-\boldsymbol{\rho}_2) + \left(1-\frac{\zeta}{z}\right)(\boldsymbol{\rho}_1'-\boldsymbol{\rho}_2')\right|. \end{aligned} \tag{4}$$

The approximate expression on the second line of Eq. 3 is derived using the method of smooth perturbations (also known as the Rytov approximation) and further assuming that Ψ is Gaussian distributed [55–57, 61–63]. We will return to Eq. 3 shortly.

The ultimate goal is to find the "two-time" MCF of a twisted space-time beam after propagating through turbulence. To do this, we must inverse Fourier transform Eq. 2, i.e.,

$$\begin{aligned} &\Gamma(\boldsymbol{\rho}_1, z, t_1, \boldsymbol{\rho}_2, z, t_2) \\ &= \iint_{-\infty}^{\infty} W(\boldsymbol{\rho}_1, z, \omega_1, \boldsymbol{\rho}_2, z, \omega_2)\exp(-\mathrm{j}\omega_1t_1)\exp(\mathrm{j}\omega_2t_2)\mathrm{d}\omega_1\mathrm{d}\omega_2. \end{aligned} \tag{5}$$

Applying Eqs 2–5 and interchanging the order of the integrals yields

$$\begin{aligned} &\Gamma(\boldsymbol{\rho}_1, z, t_1, \boldsymbol{\rho}_2, z, t_2) = \\ &\frac{1}{(2\pi)^2c^2z^2}\iiiint_{-\infty}^{\infty}\iint_{-\infty}^{\infty}\omega_1\omega_2W(\boldsymbol{\rho}_1', 0, \omega_1, \boldsymbol{\rho}_2', 0, \omega_2) \\ &\exp\left[-\frac{1}{2}D(\boldsymbol{\rho}_1'-\boldsymbol{\rho}_2', 0; \boldsymbol{\rho}_1-\boldsymbol{\rho}_2, z; \omega_1, \omega_2)\right] \\ &\exp\left[-\mathrm{j}\omega_1\left(t_1-\frac{z}{c}-\frac{|\boldsymbol{\rho}_1-\boldsymbol{\rho}_1'|^2}{2zc}\right)\right] \\ &\exp\left[\mathrm{j}\omega_2\left(t_2-\frac{z}{c}-\frac{|\boldsymbol{\rho}_2-\boldsymbol{\rho}_2'|^2}{2zc}\right)\right]\mathrm{d}\omega_1\mathrm{d}\omega_2\mathrm{d}^2\rho_1'\mathrm{d}^2\rho_2'. \end{aligned} \tag{6}$$

Assuming that the twisted space-time beam has a relatively narrow linewidth (or bandwidth) around mean or carrier frequency ω_c (i.e., $\Delta\omega/\omega_c \ll 1$), we can approximate Eq. 6 as

$$\begin{aligned} &\Gamma(\boldsymbol{\rho}_1, z, t_1, \boldsymbol{\rho}_2, z, t_2) \\ &\approx \frac{1}{\lambda_c^2z^2}\iiiint_{-\infty}^{\infty}\exp\left[-\mathrm{j}\omega_c\left(t_1-t_2-\frac{|\boldsymbol{\rho}_1-\boldsymbol{\rho}_1'|^2}{2zc}+\frac{|\boldsymbol{\rho}_2-\boldsymbol{\rho}_2'|^2}{2zc}\right)\right] \\ &\iint_{-\infty}^{\infty} W(\boldsymbol{\rho}_1', 0, \bar{\omega}_1, \boldsymbol{\rho}_2', 0, \bar{\omega}_2) \\ &\exp\left[-\frac{1}{2}D(\boldsymbol{\rho}_1'-\boldsymbol{\rho}_2', 0; \boldsymbol{\rho}_1-\boldsymbol{\rho}_2, z; \bar{\omega}_1+\omega_c, \bar{\omega}_2+\omega_c)\right] \\ &\exp\left[-\mathrm{j}\bar{\omega}_1\left(t_1-\frac{z}{c}\right)\right]\exp\left[\mathrm{j}\bar{\omega}_2\left(t_2-\frac{z}{c}\right)\right]\mathrm{d}\bar{\omega}_1\mathrm{d}\bar{\omega}_2\mathrm{d}^2\rho_1'\mathrm{d}^2\rho_2', \end{aligned} \tag{7}$$

and, by evaluating Eq. 7, obtain a closed-form expression for the MCF. Before doing this, we need to discuss the functions D and W in the integrand.

2.2 Approximate two-point, spherical WSF D

Let us return to Eq. 3. By virtue of the source being narrowband, $\beta \approx 0$. Letting Φ_n equal the von Kármán spectrum—namely,

$$\Phi_n(\kappa,\zeta) = 0.033C_n^2(\zeta)\frac{\exp(-\kappa^2/\kappa_m^2)}{(\kappa+\kappa_0^2)^{11/6}}, \tag{8}$$

where $\kappa_m = 5.92/l_0$ and $\kappa_0 = 2\pi/L_0$ (C_n^2, l_0, and L_0 are the index of refraction structure constant, the inner scale, and outer scale of turbulence, respectively)—the integral over κ evaluates to

$$\begin{aligned}D(\boldsymbol{\rho}_1'-\boldsymbol{\rho}_2',0;\boldsymbol{\rho}_1-\boldsymbol{\rho}_2,z;\omega_1,\omega_2) &= 0.033(2\pi^2)\kappa_0^{-5/3}U\left(1;\frac{1}{6};\frac{\kappa_0^2}{\kappa_m^2}\right)\\ &\times(k_1^2+k_2^2)\int_0^z C_n^2(\zeta)\mathrm{d}\zeta\\ &-0.033(4\pi^2)\kappa_0^{-5/3}k_1k_2\int_0^z C_n^2(\zeta)\\ &\times\sum_{n=0}^{\infty}\frac{(-1)^n}{n!}\left(\frac{\kappa_0^2R^2}{4}\right)^n U\left(n+1;n+\frac{1}{6};\frac{\kappa_0^2}{\kappa_m^2}\right)\mathrm{d}\zeta,\end{aligned} \tag{9}$$

where $U(a;c;z)$ is a confluent hypergeometric function of the second kind [64–66]. In most physical scenarios, $L_0 \gg l_0$, and therefore, we can estimate Eq. 9 using the small argument relation for $U(a;c;z)$. The result, after much analysis, is

$$\begin{aligned}&D(\boldsymbol{\rho}_1'-\boldsymbol{\rho}_2',0;\boldsymbol{\rho}_1-\boldsymbol{\rho}_2,z;\omega_1,\omega_2)\\ &\approx 0.7817\kappa_0^{-5/3}(k_1-k_2)^2\int_0^z C_n^2(\zeta)\mathrm{d}\zeta\\ &+8.7021\kappa_m^{-5/3}k_1k_2\int_0^z C_n^2(\zeta)\left[{}_1F_1\left(-\frac{5}{6};1;-\frac{\kappa_m^2R^2}{4}\right)-1\right]\mathrm{d}\zeta\\ &-2.3450\kappa_0^{1/3}k_1k_2\int_0^z C_n^2(\zeta)R^2\mathrm{d}\zeta.\end{aligned} \tag{10}$$

Eq. 10 includes both inner and outer scale effects. However, to evaluate Eq. 7 in closed form, we must let the inner scale $l_0 \to 0$ ($\kappa_m \to \infty$). Using the large argument relation for ${}_1F_1$, we obtain

$$\begin{aligned}D(\boldsymbol{\rho}_1'-\boldsymbol{\rho}_2',0;\boldsymbol{\rho}_1-\boldsymbol{\rho}_2,z;\omega_1,\omega_2) &\approx 0.7817\kappa_0^{-5/3}(k_1-k_2)^2\int_0^z C_n^2(\zeta)\mathrm{d}\zeta\\ &+2.9139k_1k_2\int_0^z C_n^2(\zeta)R^{5/3}\mathrm{d}\zeta-2.3450\kappa_0^{1/3}k_1k_2\int_0^z C_n^2(\zeta)R^2\mathrm{d}\zeta.\end{aligned} \tag{11}$$

We lastly assume that C_n^2 is constant over the propagation path and set $R^{5/3} \approx R^2$—an estimate known as the quadratic approximation [57, 62]. Substituting $\omega_1 = \bar{\omega}_1 + \omega_c$ and $\omega_2 = \bar{\omega}_2 + \omega_c$ as stipulated in Eq. 7 and noting that $k_1k_2 = (\bar{k}_1 + k_c)(\bar{k}_2 + k_c) \approx k_c^2$, we arrive at the final result

$$\begin{aligned}&D(\boldsymbol{\rho}_1'-\boldsymbol{\rho}_2',0;\boldsymbol{\rho}_1-\boldsymbol{\rho}_2,z;\bar{\omega}_1+\omega_c,\bar{\omega}_2+\omega_c)\\ &\approx\frac{0.7817C_n^2z\kappa_0^{-5/3}}{c^2}(\bar{\omega}_1-\bar{\omega}_2)^2+1.0930C_n^2z(1-0.7152\kappa_0^{1/3})k_c^2\\ &\left[|\boldsymbol{\rho}_1-\boldsymbol{\rho}_2|^2+|\boldsymbol{\rho}_1'-\boldsymbol{\rho}_2'|^2+(\boldsymbol{\rho}_1-\boldsymbol{\rho}_2)\cdot(\boldsymbol{\rho}_1'-\boldsymbol{\rho}_2')\right]\\ &=2\frac{a_\omega}{c^2}(\bar{\omega}_1-\bar{\omega}_2)^2\\ &+2a_sk_c^2\left[|\boldsymbol{\rho}_1-\boldsymbol{\rho}_2|^2+|\boldsymbol{\rho}_1'-\boldsymbol{\rho}_2'|^2+(\boldsymbol{\rho}_1-\boldsymbol{\rho}_2)\cdot(\boldsymbol{\rho}_1'-\boldsymbol{\rho}_2')\right].\end{aligned} \tag{12}$$

Equation 12 is very physical: The terms describe how atmospheric turbulence corrupts light's spectral and spatial coherence. For traditional space-time separable beams, these two terms give rise to pulse and beam broadening, respectively [56, 57, 67–73]. In our case, because of spatiotemporal coupling, both terms will affect the temporal and spatial beam sizes.

2.3 CSD function of a twisted space-time beam

With Eq. 12, we are one step closer to evaluating Eq. 7. We, of course, still need an expression for W. To find this expression, we begin with the MCF of a twisted space-time beam:

$$\begin{aligned}\Gamma(\boldsymbol{\rho}_1,t_1,\boldsymbol{\rho}_2,t_2) &= A^2\exp\left(-\frac{y_1^2+y_2^2}{4W_y^2}\right)\exp\left(-\frac{x_1^2+x_2^2}{4W_x^2}\right)\exp\left[-\frac{(x_1-x_2)^2}{2\delta_x^2}\right]\\ &\exp\left(-\frac{t_1^2+t_2^2}{4W_t^2}\right)\exp\left[-\frac{(t_1-t_2)^2}{2\delta_t^2}\right]\exp[\mathrm{j}\mu(x_1t_2-x_2t_1)]\exp[-\mathrm{j}\omega_c(t_1-t_2)];\end{aligned} \tag{13}$$

where A is the amplitude; W_x, W_y, and W_t are the spatial and temporal pulse widths; δ_x and δ_t are the spatial and temporal coherence widths; and μ is the space-time twist parameter [19]. The latter must satisfy $|\mu|\delta_t\delta_x \le 1$ for the MCF in Eq. 13 to be genuine, i.e., square-integrable, Hermitian, and non-negative definite [58, 59]. Consequently, $\mu \to 0$ in the coherent beam limit δ_t, $\delta_x \to \infty$. When $|\mu|\delta_t\delta_x = 1$, the twist in the beam is saturated [20, 25, 27]. We assume this condition for the simulations described in Section 3.

Note that Eq. 13 has the same general form as a twisted Gaussian Schell-model beam [22, 25–27]; however, here, space and time are twisted. It is well known that the spectral density or average irradiance of a spatially twisted random beam rotates in the x-y plane as it propagates in the z direction [35, 40, 41, 74]. From Eq. 7, we see that t is linked paraxially to the propagation distance z; therefore, a twisted space-time beam rotates or tumbles in the x-z plane as it propagates. This behavior is described in Refs. [19, 20] for twisted space-time beams propagating in free space. What remains to be determined is how atmospheric turbulence affects the x-z plane rotation of twisted space-time beams.

We can find the CSD function W of a twisted space-time beam by Fourier transforming the MCF in Eq. 13, i.e.,

$$\begin{aligned}&W(\boldsymbol{\rho}_1,\omega_1,\boldsymbol{\rho}_2,\omega_2)\\ &=\frac{1}{(2\pi)^2}\iint_{-\infty}^{\infty}\Gamma(\boldsymbol{\rho}_1,t_1,\boldsymbol{\rho}_2,t_2)\exp(\mathrm{j}\omega_1t_1)\exp(-\mathrm{j}\omega_2t_2)\mathrm{d}t_1\mathrm{d}t_2.\end{aligned} \tag{14}$$

Substituting Eq. 13 into Eq. 14 and evaluating the integrals yields

$$\begin{aligned} W(\boldsymbol{\rho}_1,\omega_1,\boldsymbol{\rho}_2,\omega_2) &= \frac{A^2}{4\pi\Omega_t}\exp\left(-\frac{y_1^2+y_2^2}{4W_y^2}\right)\exp\left(-\frac{x_1^2+x_2^2}{4\tilde{W}_x^2}\right)\exp\left[-\frac{(x_1-x_2)^2}{2\tilde{\delta}_x^2}\right] \\ &\exp\left(-\frac{\bar{\omega}_1^2+\bar{\omega}_2^2}{4W_\omega^2}\right)\exp\left[-\frac{(\bar{\omega}_1-\bar{\omega}_2)^2}{2\delta_\omega^2}\right]\exp\left\{\frac{\mu}{\delta_\omega^2}\left[\bar{\omega}_2\left(1+\frac{1}{2\gamma_t^2}\right)-\bar{\omega}_1\right]x_1\right\} \\ &\exp\left\{\frac{\mu}{\delta_\omega^2}\left[\bar{\omega}_1\left(1+\frac{1}{2\gamma_t^2}\right)-\bar{\omega}_2\right]x_2\right\}, \end{aligned} \tag{15}$$

where $\gamma_t = W_t/\delta_t$, $W_\omega = 2W_t\Omega_t$, $\delta_\omega = 2\delta_t\Omega_t$, and

$$\begin{aligned} \Omega_t^2 &= \left(\frac{1}{4W_t^2}+\frac{1}{2\delta_t^2}\right)^2-\left(\frac{1}{2\delta_t^2}\right)^2, \\ \frac{1}{\tilde{W}_x^2} &= \frac{1}{W_x^2}+\frac{\mu^2}{W_\omega^2}, \\ \frac{1}{\tilde{\delta}_x^2} &= \frac{1}{\delta_x^2}+\frac{\mu^2}{\delta_\omega^2}. \end{aligned} \tag{16}$$

With Eq. 15, we are now ready to evaluate the integrals in Eq. 7.

2.4 MCF of twisted space-time beam in atmospheric turbulence

Substituting Eqs 12, 15 into Eq. 7 and evaluating the integrals produces (after much analysis)

$$\begin{aligned} &\Gamma(x_1,0,z,t_1,x_2,0,z,t_2) \\ &= A^2\frac{W_t}{\tilde{W}_t}\frac{N_{Fx}N_{Fy}}{\sqrt{\Delta_x\Delta_y}}\exp\left[-\mathrm{j}\omega_c(\bar{t}_1-\bar{t}_2)\right] \\ &\exp\left(-\frac{N_{Fx}^2}{\Delta_x}\frac{x_1^2+x_2^2}{4W_x^2}\right)\exp\left[-\frac{\bar{t}_1^2+\bar{t}_2^2}{4\left(W_t^{\mathrm{eff}}\right)^2}\right]\exp\left[\mu\frac{N_{Fx}}{\Delta_x}\frac{W_t^2}{\tilde{W}_t^2}(x_1\bar{t}_2+x_2\bar{t}_1)\right] \\ &\exp\left[\frac{\mathrm{j}k_c}{2z}\left(1-\frac{N_{Fx}^2}{\Delta_x}+a_sk_c^2\frac{4W_x^2}{\Delta_x}\right)(x_1^2-x_2^2)\right]\exp\left[\mathrm{j}\mu^2\frac{N_{Fx}^2}{\Delta_x}\frac{W_t^2}{\tilde{W}_t^2}(\bar{t}_1^2-\bar{t}_2^2)\right] \\ &\exp\left[\mathrm{j}\mu\frac{N_{Fx}^2}{\Delta_x}\frac{W_t^2}{\tilde{W}_t^2}(x_1\bar{t}_2-x_2\bar{t}_1)\right]\exp\left[-\mathrm{j}\mu\frac{N_{Fx}^2}{\Delta_x}\frac{a_\omega}{c^2\tilde{W}_t^2}(x_1+x_2)(\bar{t}_1-\bar{t}_2)\right] \\ &\exp\left[-\mathrm{j}\mu\frac{2W_x^2}{\Delta_x}\frac{W_t^2}{\tilde{W}_t^2}a_sk_c^2(x_1-x_2)(\bar{t}_1+\bar{t}_2)\right] \\ &\exp\left[-\frac{(x_1-x_2)^2}{2\left(\delta_x^{\mathrm{eff}}\right)^2}\right]\exp\left[-\frac{(\bar{t}_1-\bar{t}_2)^2}{2\left(\delta_t^{\mathrm{eff}}\right)^2}\right]\exp\left[-\frac{(x_1-x_2)(\bar{t}_1-\bar{t}_2)}{2\left(\delta_{xt}^{\mathrm{eff}}\right)^2}\right]. \end{aligned} \tag{17}$$

Since the beam's interesting behaviors occur in the x-t or x-z plane (the x and t dimensions are coupled), here, we present the MCF evaluated at $y_1 = y_2 = 0$. The undefined symbols in Eq. 17 are $N_{Fx,y} = 2k_cW_{x,y}^2/z$, which are the x and y Fresnel numbers for a fully coherent Gaussian beam; $\bar{t} = t - z/c$ is the retarded time; $\tilde{W}_t^2 = W_t^2 + 2a_\omega/c^2$; and

$$\begin{aligned} \Delta_x &= 1+4\frac{W_x^2}{\delta_x^2}+N_{Fx}^2+8W_x^2\left(a_sk_c^2+\mu^2\frac{a_\omega}{c^2}\frac{W_t^2}{\tilde{W}_t^2}\right); \\ \Delta_y &= 1+N_{Fy}^2+8W_y^2a_sk_c^2; \\ \frac{1}{4\left(W_t^{\mathrm{eff}}\right)^2} &= \frac{1}{4\tilde{W}_t^2}+\mu^2\frac{W_x^2}{\Delta_x}\frac{W_t^4}{\tilde{W}_t^4}; \\ \frac{1}{2\left(\delta_t^{\mathrm{eff}}\right)^2} &= \frac{1}{2\delta_t^2}+\mu^2\frac{W_x^2}{2\Delta_x}\left(\Delta_x-N_{Fx}^2-\frac{W_t^4}{\tilde{W}_t^4}\right)+\frac{a_\omega}{c^2}\frac{1}{4W_t^2\tilde{W}_t^2}; \\ \frac{1}{2\left(\delta_x^{\mathrm{eff}}\right)^2} &= \frac{N_{Fx}^2}{\Delta_x}\frac{1}{2\delta_x^2}+a_sk_c^2\left(1+2\frac{N_{Fx}^2}{\Delta_x}\right)-(a_sk_c^2)^2\frac{2W_x^2}{\Delta_x^2}+\mu^2\frac{a_\omega}{c^2}\frac{N_{Fx}^2}{\Delta_x}\frac{W_t^2}{\tilde{W}_t^2}; \\ \frac{1}{2\left(\delta_{xt}^{\mathrm{eff}}\right)^2} &= \mu\frac{N_{Fx}}{2\Delta_x}\left(\Delta_x-N_{Fx}^2-\frac{W_t^2}{\tilde{W}_t^2}+a_sk_c^24W_x^2\right). \end{aligned} \tag{18}$$

Eq. 17 is organized so that the terms can be physically interpreted: Starting at the top and ignoring the carrier $\exp[-\mathrm{j}\omega_c(\bar{t}_1-\bar{t}_2)]$, the amplitude term plus the first three exponentials comprise the ensemble-averaged irradiance (discussed in more detail below). The next (complex) exponentials on line 4 are the spatial and temporal chirps. These are followed by the space-time twist on lines 5 and 6. Lastly, the exponentials on line 7 model spatial and temporal coherence.

2.5 Average irradiance and physical discussion

The ensemble-averaged irradiance is found by evaluating Eq. 17 at equal space-time points, i.e.,

$$\begin{aligned} &\langle I(x,0,z,t)\rangle = \Gamma(x,0,z,t,x,0,z,t) \\ &= A^2\frac{W_t}{\tilde{W}_t}\frac{N_{Fx}N_{Fy}}{\sqrt{\Delta_x\Delta_y}}\exp\left(-\frac{N_{Fx}^2}{\Delta_x}\frac{x^2}{2W_x^2}\right)\exp\left[-\left(1+\mu^2\frac{4W_x^2W_t^4}{\Delta_x\tilde{W}_t^2}\right)\frac{\bar{t}^2}{2\tilde{W}_t^2}\right]\exp\left(\mu\frac{2N_{Fx}}{\Delta_x}\frac{W_t^2}{\tilde{W}_t^2}x\bar{t}\right) \\ &= \hat{A}^2\exp\left(-\frac{x^2}{2\hat{W}_x^2}\right)\exp\left(-\frac{\bar{t}^2}{2\hat{W}_t^2}\right)\exp(\hat{\mu}x\bar{t}). \end{aligned} \tag{19}$$

In order, the exponentials are the spatial beam shape, temporal beam (pulse) shape, and x-t plane rotation. The behavior of the beam can be understood by examining $\hat{W}_x$, $\hat{W}_t$, and $\hat{\mu}$ *versus* Fresnel number and turbulence strength. Figure 1 shows these curves: **(A)** plots $\hat{W}_x/W_x$, $\hat{W}_t/W_t$, and $\hat{\mu}/\mu$ over Fresnel numbers ranging from 100 (near field) to 0.01 (far field). The solid, dashed, dashed-dotted, and dotted traces show how these quantities evolve in free space ($C_n^2 = 0\,\mathrm{m}^{-2/3}$) and atmospheric turbulence ($C_n^2 = 10^{-14}\,\mathrm{m}^{-2/3}$ with $L_0 = 10\,\mathrm{m}$, $50\,\mathrm{m}$, and

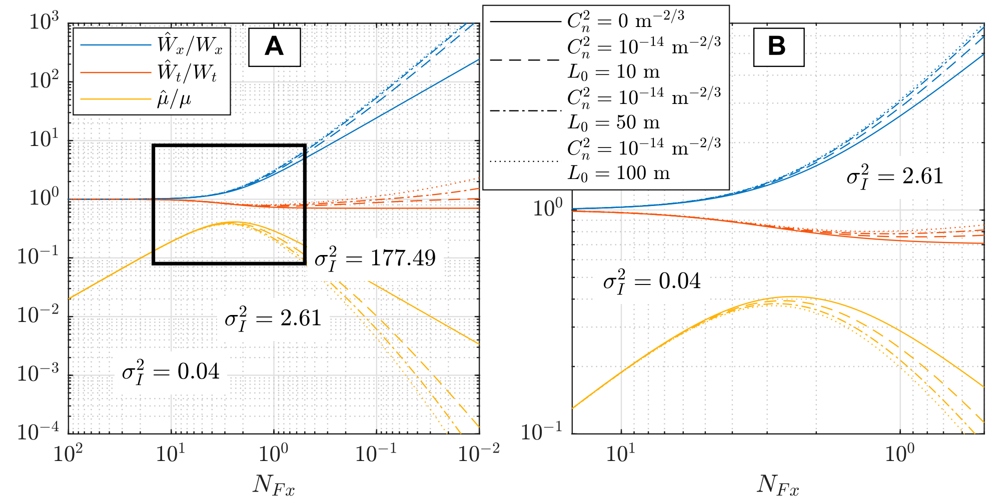

FIGURE 1
(A) $\hat{W}_x/W_x$, $\hat{W}_t/W_t$, and $\hat{\mu}/\mu$ from Eq. 19 *versus* Fresnel number N_{Fx}. **(B)** Zoomed-in view of $\hat{W}_x/W_x$, $\hat{W}_t/W_t$, and $\hat{\mu}/\mu$ over the boxed region in **(A)**. The solid, dashed, dashed-dotted, and dotted traces show the results in free space ($C_n^2 = 0$ m$^{-2/3}$) and atmospheric turbulence ($C_n^2 = 10^{-14}$ m$^{-2/3}$ with L_0=10 m, 50 m, and 100 m), respectively. The text annotations report the weak turbulence spherical wave scintillation index values σ_I^2 at the corresponding N_{Fx}. These results apply to a twisted space-time beam with parameter values equal to λ_c =1 μm, W_x =2 cm, δ_x =0.9W_x, W_t =1 ps, δ_t =0.9W_t, and $\mu = 1/(\delta_x\delta_t)$.

100 m), respectively. For the latter, the (weak turbulence) spherical wave scintillation indices [57], i.e.,

$$\sigma_I^2 = 0.5C_n^2 k_c^{7/6} z^{11/6}, \tag{20}$$

are annotated on the plot (centered on their corresponding Fresnel number) to show the strength of turbulence at that N_{Fx}. Figure 1B displays a zoomed-in view of $\hat{W}_x/W_x$, $\hat{W}_t/W_t$, and $\hat{\mu}/\mu$ over the boxed region in **(A)**, *viz.*, $15 \geq N_{Fx} \geq 0.5$. Lastly, the results depicted in Figure 1 apply to a twisted space-time beam with $\lambda_c = 1$ μm, $W_x = 2$ cm, $\delta_x = 0.9W_x$, $W_t = 1$ ps, $\delta_t = 0.9W_t$, and $\mu = 1/(\delta_x\delta_t)$.

Starting with the free-space (solid) curves in Figure 1, we see that for $N_{Fx} > 10$, the twisted space-time beam is effectively in the source plane, with $\hat{W}_x \approx W_x$, $\hat{W}_t \approx W_t$, and $\hat{\mu} < \mu/5$. Things begin to change for $10 > N_{Fx} > 1$: Most noticeably, the beam grows significantly larger due to diffraction. Indeed, over this range, the beam expands nearly three times its original size in the x direction. In addition to $\hat{W}_x$, the pulse width also changes in this region because of spatiotemporal coupling. Beginning around $N_{Fx} \approx 10$, $\hat{W}_t$ starts to contract (shorten) and continues to do so until $N_{Fx} \approx 1$. This shortening of $\hat{W}_t$ is met by an increase in $\hat{\mu}$. When considered together, the result is a beam that rotates in the x-t (or x-z) plane—the beam effectively "trades" $\hat{W}_t$ to do so. Lastly, for $N_{Fx} < 1$, $\hat{W}_x$ continues to grow larger due to diffraction, $\hat{W}_t$ asymptotes (the pulse width stops contracting), and $\hat{\mu}$ falls rapidly toward zero. Physically, the twisted space-time beam is in the far zone, diffraction dominates, and the beam no longer rotates.

Examining the turbulence (dashed, dashed-dotted, and dotted) curves, we generally observe the same behavior; however, the beam's evolution described above is effectively pushed to the left, i.e., toward higher Fresnel numbers. Where the separation between free-space (diffractive) and turbulence-induced behavior occurs (in other words, at what N_{Fx}), of course, depends on C_n^2 and L_0. Nevertheless, some general trends are evident and independent of turbulence strength:

1. The beam's size $\hat{W}_x$ asymptotically expands much more rapidly in turbulence than in free space (z^3 vice z^2) [69, 71–73].
2. After initially contracting, the pulse width $\hat{W}_t$ lengthens and continues to grow longer. While this can clearly be seen in Figure 1, more insight can be gained by examining the mathematical expression for $\hat{W}_t$, namely,

$$\frac{1}{\hat{W}_t} = \frac{1}{\tilde{W}_t}\left(1 + \mu^2 \frac{4W_x^2 W_t^4}{\Delta_x \tilde{W}_t^2}\right). \tag{21}$$

In atmospheric turbulence, the term containing the twist parameter μ tends to zero like z^{-2} (in free space, the term asymptotes to a constant value). For large z, the result is therefore $\hat{W}_t \sim \tilde{W}_t = W_t + 2a_\omega/c^2$. The turbulence contribution to the pulse width grows linearly with z [57, 67, 68], thus explaining the increasing pulse width.

3. The x-t plane rotation $\hat{\mu}$ decays much more rapidly in turbulence than in free space. Examining the mathematical relation for $\hat{\mu}$ reveals that it approaches zero like $\hat{\mu} \sim z^{-3}$ in turbulence (vice $\hat{\mu} \sim z^{-1}$ in free space) as $z \to \infty$.

3 Validation

In this section, we validate Eq. 19 by generating, in simulation, twisted space-time beam field realizations and propagating those realizations through atmospheric turbulence phase screens. Before presenting and analyzing the results, we discuss the simulation setup.

3.1 Simulation setup

3.1.1 Numbers of grid points, spacings, trials, etc.

In these wave-optics simulations, we generated and propagated twisted space-time beam field realizations through independent instances of atmospheric turbulence. The Fresnel numbers for these simulations were $N_{Fx} = 10$, 5, 2.5, and 1. For each N_{Fx}, we computed the ensemble-averaged irradiance $\langle I(x, 0, z, t)\rangle$ from 1,000 independent field and turbulence realizations. The source and observation planes were discretized using three-dimensional grids that were $N_y \times N_x \times N_t = 1,200 \times 1,200 \times 128$ with spacings equal to $\Delta_{\rm src} = 1.58$ mm, $\Delta_{\rm obs} = 2.5$ mm, and $\Delta t = 0.0781$ ps.

3.1.2 Generating twisted space-time fields

We generated twisted space-time beam field realizations using the approach described in Ref. [31]. The technique utilizes Gori and Santarsiero's integral criterion for genuine CSD functions and MCFs, colloquially known as the superposition rule [75, 76]. Specialized for our purposes, a thermal (or pseudo-thermal) twisted space-time beam field realization can be generated by evaluating the following superposition integral:

$$U(\boldsymbol{\rho}, t) = \iint_{-\infty}^{\infty} r(v_x, v_t)\sqrt{\frac{1}{2}p(v_x, v_t)}H(\boldsymbol{\rho}, t; v_x, v_t)\mathrm{d}v_x\mathrm{d}v_t, \quad (22)$$

where r is a zero-mean, unit-variance, delta-correlated, complex Gaussian random function [31], and p and H are

$$\begin{aligned} p(v_x, v_t) &= \sqrt{\frac{\alpha}{\pi}}\exp(-\alpha v_x^2)\sqrt{\frac{\beta}{\pi}}\exp(-\beta v_t^2) \\ H(\boldsymbol{\rho}, t; v_x, v_t) &= A\exp\left(-\frac{y^2}{4W_y^2}\right)\exp(-\sigma_x x^2)\exp(-\sigma_t t^2) \\ &\quad \exp[\mathrm{j}(x - \mathrm{j}\alpha\mu t)v_x]\exp[\mathrm{j}(t + \mathrm{j}\beta\mu x)v_t]. \end{aligned} \quad (23)$$

The α, β, σ_x, and σ_t relate to the physical twisted space-time beam parameters in Eq. 13 *via* the relations [19, 35].

$$\begin{aligned} \frac{1}{4W_x^2} &= \sigma_x - \frac{\beta\mu^2}{2}, \quad \frac{1}{4W_t^2} = \sigma_t - \frac{\alpha\mu^2}{2}, \\ \frac{1}{2\delta_x^2} &= \frac{\beta\mu^2}{4} + \frac{1}{4\alpha}, \quad \frac{1}{2\delta_t^2} = \frac{\alpha\mu^2}{4} + \frac{1}{4\beta}. \end{aligned} \quad (24)$$

In the simulations, we produced twisted space-time beams with the following parameter values $\lambda_c = 1\ \mu$m, $W_x = W_y = 2$ cm, $\delta_x = 0.9W_x$, $W_t = 1$ ps, $\delta_t = 0.9W_t$, and $\mu = 1/(\delta_x\delta_t)$—the same as in Figure 1. These parameter values corresponded to $\alpha = 3.24$ cm^2, $\beta = 0.81$ ps^2, $\sigma_x = 0.2168$ cm^{-2}, and $\sigma_t = 0.8673$ ps^{-2}. We evaluated Eq. 22 as a matrix-vector product, where the v_x and v_t dimensions were discretized using 64 grid points each, with spacings equal to $\Delta v_x = 0.0645$ cm^{-1} and $\Delta v_t = 0.1291$ ps^{-1}, respectively.

3.1.3 Atmospheric turbulence

The index of refraction structure constant and outer scale for the atmospheric turbulence was $C_n^2 = 10^{-14}$ m$^{-2/3}$ and $L_0 = 10$ m, corresponding to the dashed traces in Figure 1. We simulated propagation through this turbulence using the split-step algorithm described in Refs. [70, 77–80]. For $N_{Fx} = 10$, 5, 2.5, and 1, we discretized the continuous propagation paths using 4, 5, 9, and 20 equally spaced, statistically independent phase screens generated using the Fourier transform (also known as the spectral) method and augmented with subharmonics [70, 78, 81, 82]. The strength of each phase screen (C_n^2, Fried's parameter r_0, or coherence width ρ_0) was selected such that the discrete-path spherical wave r_0 and scintillation index σ_I^2 matched those of the desired, continuous turbulent path. To capture the change in phase due to turbulence over the light source's bandwidth, we divided each phase screen by k_c to convert from radians to meters of optical path length (OPL).

Note that we did not simulate the other turbulence conditions reported in Figure 1 due to computational constraints. Accurately simulating turbulence with a given outer scale requires phase screens that have physical dimensions on the order of L_0. Simulating the $L_0 = 50$ m and 100 m atm would have required grids that were (approximately) 25 and 100 times larger (in numbers of points), respectively, than those used in the $L_0 = 10$ m simulations (see Section 3.1.1).

3.1.4 Procedure

On each Monte Carlo trial,

1. We generated a twisted space-time beam realization and an instance of atmospheric turbulence as described above.

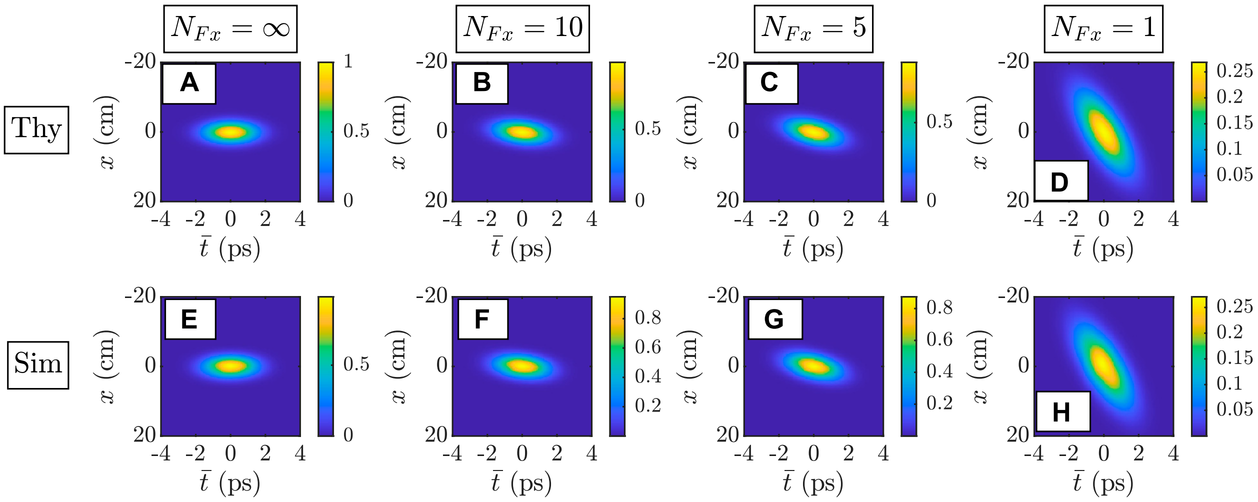

FIGURE 2
Ensemble-averaged irradiance $\langle I(x,0,z,t)\rangle$ free-space results: **(A)** theory $N_{Fx} = \infty$, **(B)** theory $N_{Fx} = 10$, **(C)** theory $N_{Fx} = 5$, **(D)** theory $N_{Fx} = 1$, **(E)** simulation $N_{Fx} = \infty$, **(F)** simulation $N_{Fx} = 10$, **(G)** simulation $N_{Fx} = 5$, and **(H)** simulation $N_{Fx} = 1$.

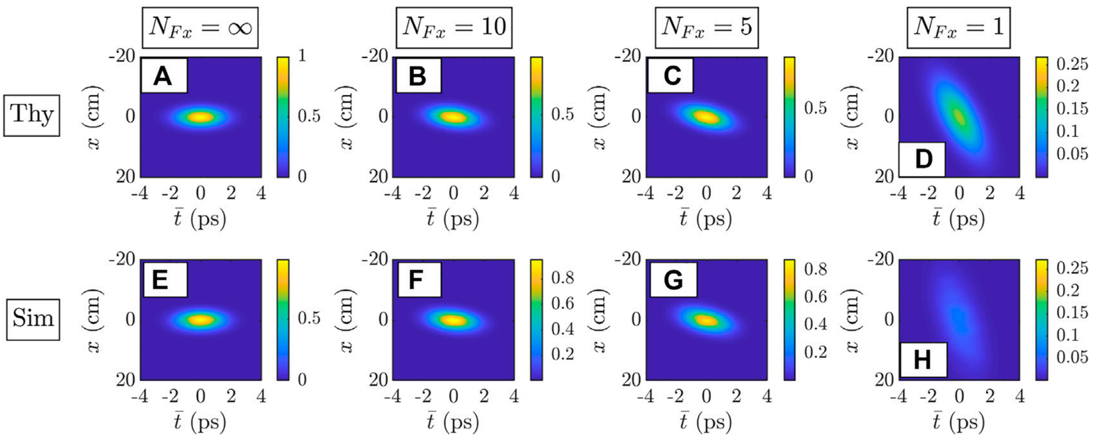

FIGURE 3
Ensemble-averaged irradiance $\langle I(x,0,z,t)\rangle$ turbulence results: **(A)** theory $N_{Fx} = \infty$, **(B)** theory $N_{Fx} = 10$, **(C)** theory $N_{Fx} = 5$, **(D)** theory $N_{Fx} = 1$, **(E)** simulation $N_{Fx} = \infty$, **(F)** simulation $N_{Fx} = 10$, **(G)** simulation $N_{Fx} = 5$, and **(H)** simulation $N_{Fx} = 1$.

2. We then Fourier transformed the twisted space-time beam realization to the ω domain using a fast Fourier transform (FFT) computed along the third dimension of U.
3. We propagated U to each of the 4, 5, 9, or 20 (depending on N_{Fx}) planes using the convolution form of the Fresnel diffraction integral (also known as the angular spectrum propagation method [78, 80]), which we evaluated using FFTs computed along U's spatial dimensions.
4. In each plane, we converted the atmospheric phase screen in meters of OPL to radians using the ω values along the third dimension of U. We then applied the phase screen to the field and propagated U to the next plane.
5. Upon reaching the observation plane, we Fourier transformed the field back to the t domain using an FFT computed along U's third dimension.
6. Lastly, we computed the trial irradiance $I(x,0,z,t) = |U(x,0,z,t)|^2$.

We repeated this procedure 1,000 times.

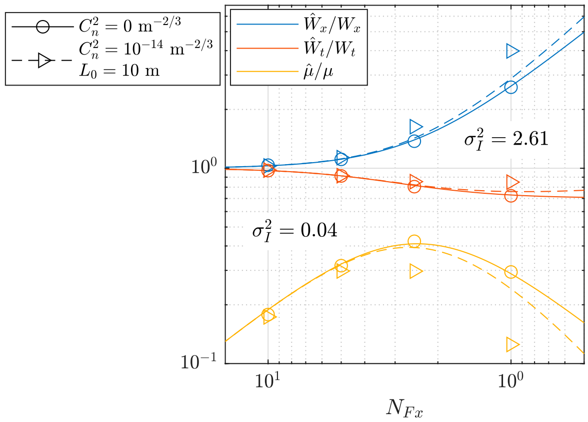

FIGURE 4
Theory [Eq. 19] and simulation $\hat{W}_x/W_x$, $\hat{W}_t/W_t$, and $\hat{\mu}/\mu$ *versus* Fresnel number N_{Fx}. The symbols ∘ and ▹ are the results of the simulation.

3.2 Results

Figures 2–4 show the results of the twisted space-time beam simulations. Figures 2, 3—which report the ensemble-averaged irradiances $\langle I(x,0,z,t)\rangle$ after propagating through free space (included as a reference) and atmospheric turbulence, respectively—are organized in the same manner: The top row shows the theoretical $\langle I(x,0,z,t)\rangle$ given in Eq. 19 for Fresnel numbers $N_{Fx} = \infty$, 10, 5, and 1, respectively. The bottom (second) row displays the same for the simulated $\langle I(x,0,z,t)\rangle$. The images in Figure 3 are encoded using the same color scales as the corresponding subfigures in Figure 2. Row and column headings have been added to both figures to aid the reader. Lastly, Figure 4 reports the theoretical and simulated $\hat{W}_x/W_x$, $\hat{W}_t/W_t$, and $\hat{\mu}/\mu$ *versus* Fresnel number N_{Fx}. The solid and dashed curves in the figure are the same as those shown in Figure 1B; however, here, we have added the simulated results denoted by the markers ∘ and ▹. We obtained these results by fitting Gaussian functions to the simulated $\langle I(x,0,z,t)\rangle$.

Inspection of Figure 3 reveals good agreement between simulation and theory in weak to moderately strong atmospheric turbulence [Figures 3B, C, F, and G]. In contrast, the agreement is rather poor in strong turbulence [Figures 3D, H]. This discrepancy is likely caused by the quadratic approximation we used to derive the MCF in Eq. 17 and subsequently $\langle I(x,0,z,t)\rangle$ in Eq. 19. The validity of the quadratic approximation (and the extended Huygens–Fresnel principle, more generally) is suspect in strong turbulence [61–63, 83]. Thus, the disagreement in Figures 3D, H is somewhat expected. The results in Figure 4 are consistent with those in Figure 3—we observe good agreement in weak-to-moderate turbulence and poor agreement in strong turbulence. Although the theoretical relations for $\hat{W}_x/W_x$, $\hat{W}_t/W_t$, and $\hat{\mu}/\mu$ generally underestimate the effects of turbulence on those parameters, they do accurately predict the trends *versus* Fresnel number and turbulence strength.

3.3 Experimental verification

Before concluding, we briefly discuss the process for experimentally verifying the theoretical and simulated results presented above. Twisted space-time beam field realizations can be physically synthesized using an apparatus known as a Fourier transform pulse shaper (FTPS) [1, 4, 9, 84–87]. An FTPS consists of two identical gratings separated by a 4*f* cylindrical lens (CL) system. At the center of the 4*f* system is a spatial light modulator (SLM). Assuming a pulsed laser beam is input into the FTPS, the first grating-CL-2*f* system spreads and maps the input beam's spectrum into physical space at the SLM plane. The SLM modifies the field in the space-frequency (x-ω) domain, which is then transformed back to the space-time domain by the second grating-CL-2*f* system. Partial coherence manifests by incoherently summing many independent twisted space-time beam realizations.

Turbulence (besides outdoor experiments which are generally uncontrolled) can be controllably generated in the laboratory using several different methods [88]. Of these, phase plate/wheel [89–92] or hot-air [93, 94] techniques are the most germane, and systems employing those methods are easily capable of reproducing the turbulence conditions simulated above.

Lastly, to observe the beam's behavior in x-t domain, we follow the procedure described in Refs. [1, 5]: The light at the output of the turbulence generator transits a grating-CL-2*f* system and then is measured by a detector. The detector measures the light's spatially resolved spectrum averaged over many independent field and turbulence realizations, i.e.,

$$S(x,z,\omega) = \langle |U(x,z,\omega)|^2 \rangle. \tag{25}$$

Note that this quantity is also referred to as the spectral density [58, 59, 71, 72]. Using Eq. 14, the spectral density relates to the MCF *via*

$$S(x,z,\omega) = \frac{1}{(2\pi)^2} \iint_{-\infty}^{\infty} \Gamma(x,z,t_1,x,z,t_2) \exp[j\omega(t_1-t_2)] \mathrm{d}t_1 \mathrm{d}t_2, \tag{26}$$

and consequently, the ensemble-averaged irradiance $\langle I(x,z,t) \rangle$ is not directly recoverable. Likely, the easiest course of action is to compare the measured spectral density to its theoretical and simulated counterparts to validate the latter.

4 Conclusion

In this paper, we focused on a recently introduced, partially coherent, space-time-coupled field known as a twisted space-time beam. Twisted space-time beams are similar to traditional twisted Gaussian Schell-model beams; however, instead of being spatially twisted (like the latter), the former possess a stochastic twist which couples their space and time dimensions. Like STOV beams, this spatiotemporal twist imbues twisted space-time beams with transverse (to the direction of propagation) angular momentum.

Generalizing the original research presented in Refs. [19, 20], here, we studied how twisted space-time beams behave as they propagate through atmospheric turbulence. Applying the extended Huygens–Fresnel principle, we derived the MCF for twisted space-time beams after propagating a distance z through atmospheric turbulence of arbitrary strength. From the MCF, we obtained the ensemble-averaged irradiance and quantified the effects of turbulence on beam size, pulse width, and space-time twist. We then simulated twisted space-time beam propagation through atmospheric turbulence to validate our theoretical analysis. The simulated results were found to be in good agreement with theory in weak-to-moderate turbulence. On the other hand, we observed rather poor agreement in strong turbulence, where our theoretical expression for the ensemble-averaged irradiance underestimated the effects of turbulence on the beam size, pulse width, and space-time twist. It did, however, accurately predict the trends of those parameters *versus* Fresnel number and turbulence strength.

Light with engineered space-time or spatiotemporal coupling is a new and exciting aspect of beam control research, with potential revolutionary uses in optical communications, optical tweezing, and quantum optics. While the free-space propagation characteristics of space-time-coupled beams are generally understood, much less is known about how these beams behave in random media. The results in this paper are a first step toward this goal.

Data availability statement

The original contributions presented in the study are included in the article/Supplementary Material, further inquiries can be directed to the corresponding author.

Author contributions

MH performed the tasks of conceptualization, formal analysis, investigation, methodology, validation, visualization, and writing.

Acknowledgments

The views expressed in this paper are those of the authors and do not reflect the official policy or position of the US Air Force, the Department of Defense, or the US government. MH would like to thank the Air Force Office of Scientific Research (AFOSR) Physical and Biological Sciences Branch (RTB) for supporting this work.

Conflict of interest

The author declares that the research was conducted in the absence of any commercial or financial relationships that could be construed as a potential conflict of interest.

Publisher's note

References

1. Kondakci HE, Abouraddy AF. Diffraction-free space-time light sheets. *Nat Photon* (2017) 11:733–40. doi:10.1038/s41566-017-0028-9

2. Yessenov M, Bhaduri B, Kondakci HE, Abouraddy AF. Weaving the rainbow: Space-time optical wave packets. *Opt. Photonics News* (2019) 30(5):34–41. doi:10.1364/OPN.30.5.000034

3. Bhaduri B, Yessenov M, Abouraddy AF. Anomalous refraction of optical spacetime wave packets. *Nat Photon* (2020) 14:416–21. doi:10.1038/s41566-020-0645-6

4. Yessenov M, Hall LA, Schepler KL, Abouraddy AF. Space-time wave packets. *Adv Opt Photon* (2022) 14:455–570. doi:10.1364/AOP.450016

5. Dallaire M, McCarthy N, Piché M. Spatiotemporal bessel beams: Theory and experiments. *Opt Express* (2009) 17:18148–64. doi:10.1364/OE.17.018148

6. Bliokh KY, Nori F. Spatiotemporal vortex beams and angular momentum. *Phys Rev A (Coll Park)* (2012) 86:033824. doi:10.1103/PhysRevA.86.033824

7. Jhajj N, Larkin I, Rosenthal EW, Zahedpour S, Wahlstrand JK, Milchberg HM. Spatiotemporal optical vortices. *Phys Rev X* (2016) 6:031037. doi:10.1103/PhysRevX.6.031037

8. Hancock SW, Zahedpour S, Goffin A, Milchberg HM. Free-space propagation of spatiotemporal optical vortices. *Optica* (2019) 6:1547–53. doi:10.1364/OPTICA.6.001547

9. Chong A, Wan C, Chen J, Zhan Q. Generation of spatiotemporal optical vortices with controllable transverse orbital angular momentum. *Nat Photon* (2020) 14:350–4. doi:10.1038/s41566-020-0587-z

10. Meng X, Hu Y, Wan C, Zhan Q. Optical vortex fields with an arbitrary orbital angular momentum orientation. *Opt Lett* (2022) 47:4568–71. doi:10.1364/OL.468360

11. Wan C, Chen J, Chong A, Zhan Q. Photonic orbital angular momentum with controllable orientation. *Natl Sci Rev* (2021) 9:nwab149. doi:10.1093/nsr/nwab149

12. Yao AM, Padgett MJ. Orbital angular momentum: Origins, behavior and applications. *Adv Opt Photon* (2011) 3:161–204. doi:10.1364/AOP.3.000161

13. Gao D, Ding W, Nieto-Vesperinas M, Ding X, Rahman M, Zhang T, et al. Optical manipulation from the microscale to the nanoscale: Fundamentals, advances and prospects. *Light Sci Appl* (2017) 6:e17039. doi:10.1038/lsa.2017.39

14. Padgett MJ. Orbital angular momentum 25 years on [Invited]. *Opt Express* (2017) 25:11265–74. doi:10.1364/OE.25.011265

15. Shen Y, Wang X, Xie Z, Min C, Fu X, Liu Q, et al. Optical vortices 30 years on: OAM manipulation from topological charge to multiple singularities. *Light Sci Appl* (2019) 8:90. doi:10.1038/s41377-019-0194-2

16. Angelsky OV, Bekshaev AY, Hanson SG, Zenkova CY, MokhunII, Jun Z. Structured light: Ideas and concepts. *Front Phys* (2020) 8:114. doi:10.3389/fphy.2020.00114

17. Yessenov M, Bhaduri B, Kondakci HE, Meem M, Menon R, Abouraddy AF. Non-diffracting broadband incoherent space-time fields. *Optica* (2019) 6:598–607. doi:10.1364/OPTICA.6.000598

18. Mirando A, Zang Y, Zhan Q, Chong A. Generation of spatiotemporal optical vortices with partial temporal coherence. *Opt Express* (2021) 29:30426–35. doi:10.1364/OE.431882

19. Hyde MW. Twisted space-frequency and space-time partially coherent beams. *Sci Rep* (2020) 10:12443. doi:10.1038/s41598-020-68705-9

20. Hyde IVMW. Twisted spatiotemporal optical vortex random fields. *IEEE Photon J* (2021) 13:1–16. doi:10.1109/JPHOT.2021.3066898

21. Ding C, Horoshko D, Korotkova O, Jing C, Qi X, Pan L. Source coherence-induced control of spatiotemporal coherency vortices. *Opt Express* (2022) 30:19871. doi:10.1364/OE.458666

22. Simon R, Mukunda N. Twisted Gaussian schell-model beams. *J Opt Soc Am A* (1993) 10:95–109. doi:10.1364/JOSAA.10.000095

23. Simon R, Sundar K, Mukunda N. Twisted Gaussian Schell-model beams. I. Symmetry structure and normal-mode spectrum. *J Opt Soc Am A* (1993) 10:2008. doi:10.1364/JOSAA.10.002008

24. Sundar K, Simon R, Mukunda N. Twisted Gaussian Schell-model beams. II. Spectrum analysis and propagation characteristics. *J Opt Soc Am A* (1993) 10:2017–23. doi:10.1364/JOSAA.10.002017

25. Simon R, Mukunda N. Twist phase in Gaussian-beam optics. *J Opt Soc Am A* (1998) 15:2373–82. doi:10.1364/JOSAA.15.002373

26. Ambrosini D, Bagini V, Gori F, Santarsiero M. Twisted Gaussian schell-model beams: A superposition model. *J Mod Opt* (1994) 41:1391–9. doi:10.1080/09500349414551331

27. Gori F, Santarsiero M, Borghi R, Vicalvi S. Partially coherent sources with helicoidal modes. *J Mod Opt* (1998) 45:539–54. doi:10.1080/09500349808231913

28. Friberg AT, Tervonen E, Turunen J. Interpretation and experimental demonstration of twisted Gaussian Schell-model beams. *J Opt Soc Am A* (1994) 11:1818–26. doi:10.1364/JOSAA.11.001818

29. Wang H, Peng X, Liu L, Wang F, Cai Y, Ponomarenko SA. Generating bona fide twisted Gaussian Schell-model beams. *Opt Lett* (2019) 44:3709–12. doi:10.1364/OL.44.003709

30. Tian C, Zhu S, Huang H, Cai Y, Li Z. Customizing twisted Schell-model beams. *Opt Lett* (2020) 45:5880–3. doi:10.1364/OL.405149

31. Hyde MW. Stochastic complex transmittance screens for synthesizing general partially coherent sources. *J Opt Soc Am A* (2020) 37:257–64. doi:10.1364/JOSAA.381772

32. Wang H, Peng X, Zhang H, Liu L, Chen Y, Wang F, et al. Experimental synthesis of partially coherent beam with controllable twist phase and measuring its orbital angular momentum. *Nanophotonics* (2021) 11:689–96. doi:10.1515/nanoph-2021-0432

33. Zhang Y, Zhang X, Wang H, Ye Y, Liu L, Chen Y, et al. Generating a twisted Gaussian Schell-model beam with a coherent-mode superposition. *Opt Express* (2021) 29:41964–74. doi:10.1364/OE.446160

34. Gori F, Santarsiero M. Twisted Gaussian Schell-model beams as series of partially coherent modified Bessel-Gauss beams. *Opt Lett* (2015) 40:1587–90. doi:10.1364/OL.40.001587

35. Mei Z, Korotkova O. Random sources for rotating spectral densities. *Opt Lett* (2017) 42:255–8. doi:10.1364/OL.42.000255

36. Borghi R. Twisting partially coherent light. *Opt Lett* (2018) 43:1627–30. doi:10.1364/OL.43.001627

37. Gori F, Santarsiero M. Devising genuine twisted cross-spectral densities. *Opt Lett* (2018) 43:595–8. doi:10.1364/OL.43.000595

38. Serna J, Movilla JM. Orbital angular momentum of partially coherent beams. *Opt Lett* (2001) 26:405–7. doi:10.1364/OL.26.000405

39. Kim SM, Gbur G. Angular momentum conservation in partially coherent wave fields. *Phys Rev A (Coll Park)* (2012) 86:043814. doi:10.1103/PhysRevA.86.043814

40. Gbur GJ. *Singular optics*. Boca Raton, FL: CRC Press (2016).

41. Stahl CSD, Gbur G. Twisted vortex Gaussian Schell-model beams. *J Opt Soc Am A* (2018) 35:1899–906. doi:10.1364/JOSAA.35.001899

42. Lin Q, Cai Y. Tensor ABCD law for partially coherent twisted anisotropic Gaussian-Schell model beams. *Opt Lett* (2002) 27:216–8. doi:10.1364/OL.27.000216

43. Cai Y, He S. Propagation of a partially coherent twisted anisotropic Gaussian Schell-model beam in a turbulent atmosphere. *Appl Phys Lett* (2006) 89:041117. doi:10.1063/1.2236463

44. Wang F, Cai Y. Second-order statistics of a twisted Gaussian Schell-model beam in turbulent atmosphere. *Opt Express* (2010) 18:24661–72. doi:10.1364/OE.18.024661

45. Wang F, Cai Y, Eyyuboğlu HT, Baykal Y. Twist phase-induced reduction in scintillation of a partially coherent beam in turbulent atmosphere. *Opt Lett* (2012) 37:184–6. doi:10.1364/OL.37.000184

46. Cai Y, Zhu S. Orbital angular moment of a partially coherent beam propagating through an astigmatic ABCD optical system with loss or gain. *Opt Lett* (2014) 39:1968. doi:10.1364/ol.39.001968

47. Charnotskii M. Transverse linear and orbital angular momenta of beam waves and propagation in random media. *J Opt* (2018) 20:025602. doi:10.1088/2040-8986/aa9f50

48. Wang J, Wang H, Zhu S, Li Z. Second-order moments of a twisted Gaussian Schell-model beam in anisotropic turbulence. *J Opt Soc Am A* (2018) 35:1173–9. doi:10.1364/JOSAA.35.001173

49. Zhou M, Fan W, Wu G. Evolution properties of the orbital angular momentum spectrum of twisted Gaussian Schell-model beams in turbulent atmosphere. *J Opt Soc Am A* (2020) 37:142–8. doi:10.1364/JOSAA.37.000142

50. Liu Z, Wan L, Zhou Y, Zhang Y, Zhao D. Progress on studies of beams carrying twist. *Photonics* (2021) 8:92. doi:10.3390/photonics8040092

51. Ponomarenko SA. Classical entanglement of twisted random light propagating through atmospheric turbulence [Invited]. *J Opt Soc Am A* (2022) 39:C1. C1–C5. doi:10.1364/JOSAA.465410

52. Bliokh KY. Spatiotemporal vortex pulses: Angular momenta and spin-orbit interaction. *Phys Rev Lett* (2021) 126:243601. doi:10.1103/PhysRevLett.126.243601

53. Hancock SW, Zahedpour S, Milchberg HM. Mode structure and orbital angular momentum of spatiotemporal optical vortex pulses. *Phys Rev Lett* (2021) 127:193901. doi:10.1103/PhysRevLett.127.193901

54. Lutomirski RF, Yura HT. Propagation of a finite optical beam in an inhomogeneous medium. *Appl Opt* (1971) 10:1652–8. doi:10.1364/AO.10.001652

55. Fante RL, Wolf E. VI wave propagation in random media: A system approach. *Opt (Elsevier), Prog Opt* (1985) 22:341–98. chap. 6. doi:10.1016/S0079-6638(08)70152-5

56. Ishimaru A. *Wave propagation and scattering in random media*. Piscataway, NJ: IEEE Press (1999). p. 600.

57. Andrews LC, Phillips RL. *Laser beam propagation through random media*. 2nd ed. Bellingham, WA: SPIE Press (2005).

58. Mandel L, Wolf E. *Optical coherence and quantum optics*. New York, NY: Cambridge University (1995).

59. Lajunen H, Vahimaa P, Tervo J. Theory of spatially and spectrally partially coherent pulses. *J Opt Soc Am A* (2005) 22:1536–45. doi:10.1364/josaa.22.001536

60. Fante R. Electromagnetic beam propagation in turbulent media. *Proc IEEE* (1975) 63:1669–92. doi:10.1109/PROC.1975.10035

61. Fante R. Electromagnetic beam propagation in turbulent media: An update. *Proc IEEE* (1980) 68:1424–43. doi:10.1109/PROC.1980.11882

62. Fante RL. Two-position, two-frequency mutual-coherence function in turbulence. *J Opt Soc Am* (1981) 71:1446–51. doi:10.1364/JOSA.71.001446

63. Charnotskii M. Extended huygens-fresnel principle and optical waves propagation in turbulence: Discussion. *J Opt Soc Am A* (2015) 32:1357–65. doi:10.1364/JOSAA.32.001357

64. M Abramowitz IA Stegun, editors. *Handbook of mathematical functions with formulas, graphs, and mathematical tables*. Washington, DC: National Bureau of Standards (1964).

65. Gradshteyn IS, Ryzhik IM. *Table of integrals, series, and products*. 7th ed. Burlington, MA: Academic Press (2007).

66. Belafhal A, Chib S, Khannous F, Usman T. Evaluation of integral transforms using special functions with applications to biological tissues. *Comp Appl Math* (2021) 40:156. doi:10.1007/s40314-021-01542-2

67. Young CY, Andrews LC, Ishimaru A. Time-of-arrival fluctuations of a space–time Gaussian pulse in weak optical turbulence: An analytic solution. *Appl Opt* (1998) 37:7655–60. doi:10.1364/AO.37.007655

68. Young CY. Broadening of ultrashort optical pulses in moderate to strong turbulence. In: JC Ricklin DG Voelz, editors. *Free-space laser communication and laser imaging II*, 4821. Seattle, Washington, USA: International Society for Optics and Photonics SPIE (2002). p. 74–81. doi:10.1117/12.452061

69. Gbur G, Wolf E. Spreading of partially coherent beams in random media. *J Opt Soc Am A* (2002) 19:1592–8. doi:10.1364/JOSAA.19.001592

70. Gbur G. Partially coherent beam propagation in atmospheric turbulence [Invited]. *J Opt Soc Am A* (2014) 31:2038–45. doi:10.1364/JOSAA.31.002038

71. Korotkova O. *Random light beams: Theory and applications*. Boca Raton, FL: CRC (2014).

72. Korotkova O. *Theoretical statistical optics*. Hackensack, NJ: World Scientific (2021).

73. Wang F, Liu X, Cai Y. Propagation of partially coherent beam in turbulent atmosphere: A review (invited review). *Prog Electromagn Res* (2015) 150:123–43. doi:10.2528/PIER15010802

74. Wan L, Zhao D. Controllable rotating Gaussian Schell-model beams. *Opt Lett* (2019) 44:735–8. doi:10.1364/OL.44.000735

75. Gori F, Santarsiero M. Devising genuine spatial correlation functions. *Opt Lett* (2007) 32:3531–3. doi:10.1364/OL.32.003531

76. Martínez-Herrero R, Mejías PM, Gori F. Genuine cross-spectral densities and pseudo-modal expansions. *Opt Lett* (2009) 34:1399–401. doi:10.1364/OL.34.001399

77. Martin JM, Flatté SM. Intensity images and statistics from numerical simulation of wave propagation in 3-D random media. *Appl Opt* (1988) 27:2111–26. doi:10.1364/AO.27.002111

78. Schmidt JD. *Numerical simulation of optical wave propagation with examples in MATLAB*. Bellingham, WA: SPIE Press (2010).

79. Jarem JM, Banerjee PP. *Computational methods for electromagnetic and optical systems*. 2nd ed. Boca Raton, FL: CRC Press (2011).

80. Voelz DG. *Computational fourier optics: A matlab tutorial*. Bellingham, WA: SPIE (2011).

81. Lane RG, Glindemann A, Dainty JC. Simulation of a Kolmogorov phase screen. *Waves in Random Media* (1992) 2:209–24. doi:10.1088/0959-7174/2/3/003

82. Frehlich R. Simulation of laser propagation in a turbulent atmosphere. *Appl Opt* (2000) 39:393–7. doi:10.1364/AO.39.000393

83. Fante RL. Some physical insights into beam propagation in strong turbulence. *Radio Sci* (1980) 15:757–62. doi:10.1029/RS015i004p00757

84. Weiner AM. Femtosecond pulse shaping using spatial light modulators. *Rev Sci Instrum* (2000) 71:1929–60. doi:10.1063/1.1150614

85. Ding C, Koivurova M, Turunen J, Setälä T, Friberg AT. Coherence control of pulse trains by spectral phase modulation. *J Opt* (2017) 19:095501. doi:10.1088/2040-8986/aa7b5e

86. Goodman JW. *Introduction to fourier optics*. 3rd ed. Englewood, CO: Roberts & Company (2005).

87. Torres-Company V, Lancis J, Andrés P. Space-time analogies in optics. In: E Wolf, editor. *Prog. Opt.*, 56. Elsevier (2011). p. 1–80. chap. 1. doi:10.1016/B978-0-444-53886-4.00001-0

88. Jolissaint L. Optical turbulence generators for testing astronomical adaptive optics systems: A review and designer guide. *Publ Astron Soc Pac* (2006) 118:1205–24. doi:10.1086/507849

89. Rodenburg B, Mirhosseini M, Malik M, Magaña-Loaiza OS, Yanakas M, Maher L, et al. Simulating thick atmospheric turbulence in the lab with application to orbital angular momentum communication. *New J Phys* (2014) 16:033020. doi:10.1088/1367-2630/16/3/033020

90. Rickenstorff C, Rodrigo JA, Alieva T. Programmable simulator for beam propagation in turbulent atmosphere. *Opt Express* (2016) 24:10000–12. doi:10.1364/OE.24.010000

91. Dayton D, Spencer M, Hassall A, Rhoadarmer T. Distributed-volume optical disturbance generation in a scaled-laboratory environment using nematic liquid-crystal phase modulators. In: JJ Dolne PJ Bones, editors. *Unconventional and indirect imaging, image reconstruction, and wavefront sensing 2018*, 10772. San Diego, California, USA: International Society for Optics and Photonics SPIE (2018). p. 107720H. doi:10.1117/12.2319968

92. Joo JY, Han SG, Lee JH, Rhee HG, Huh J, Lee K, et al. Development and characterization of an atmospheric turbulence simulator using two rotating phase plates. *Curr Opt Photon* (2022) 6:445–52.

93. Keskin O, Jolissaint L, Bradley C. Hot-air optical turbulence generator for the testing of adaptive optics systems: Principles and characterization. *Appl Opt* (2006) 45:4888–97. doi:10.1364/AO.45.004888

94. DiComo G, Helle M, Peñano J, Ting A, Schmitt-Sody A, Elle J. Implementation of a long range, distributed-volume, continuously variable turbulence generator. *Appl Opt* (2016) 55:5192–7. doi:10.1364/AO.55.005192